Diffusive evolution of experimental braided rivers

M. D. Reitz, D. J. Jerolmack, E. Lajeunesse, Angela Limare, O. Devauchelle, F. Métivier

Diffusive evolution of experimental braided rivers

Meredith D. Reitz,[1,*] Douglas J. Jerolmack,[2] Eric Lajeunesse,[3] Angela Limare,[3] Olivier Devauchelle,[3] and François Métivier[3]

[1]*Lamont-Doherty Earth Observatory, Columbia University, Palisades, New York, USA*

[2]*Department of Earth and Environmental Science, University of Pennsylvania, Philadelphia, Pennsylvania, USA*

[3]*Equipe de Dynamique des Fluides Geologiques, Institut de Physique du Globe de Paris, Paris, France*

(Received 4 October 2013; revised manuscript received 6 March 2014; published 15 May 2014)

Water flowing over a loose granular bed organizes into a braided river, a network of ephemeral and interacting channels. The temporal and spatial evolution of this network of braided channels is not yet quantitatively understood. In ∼1 m-scale experiments, we found that individual channels exhibit a self-similar geometry and near-threshold transport conditions. Measurements of the rate of growth of topographic correlation length scales, the time scale of system-slope establishment, and the random spatial decorrelation of channel locations indicate together that the evolution of the braided river system may be diffusive in nature. This diffusion is due to the separation of scales between channel formation and network evolution, and the random motion of interacting channels when viewed at a coarse-grained scale.

DOI: 10.1103/PhysRevE.89.052809 PACS number(s): 05.65.+b, 92.40.Gc, 05.40.−a, 47.27.W−

I. INTRODUCTION

In the absence of lateral confinement or cohesion effects, water-transported sediment creates a braided river: a network of channels that exhibit rapid creation, migration, and abandonment dynamics (Fig. 1) [1–4]. Despite the complex appearance and erratic dynamics of braided rivers, decades of laboratory experiments and field observations have documented order in the structure of the channel network [3,5–12]. The processes at the scale of individual channels that drive their formation and movement have also been identified [5,13–18] and were used to inform a cellular numerical model of water routing and sediment transport that qualitatively reproduced braided river morphology and dynamics [2]. Yet some of the most basic questions about these systems remain unanswered: Do the individual channels exhibit equilibrium geometry, and if so what sets this equilibrium? How do channels migrate through space to evolve the network? And how are the unit- and system-scale (channel and channel-network scale) processes related?

Theory and observation have confirmed that single-channel (nonbraided) rivers with gravel beds exhibit an equilibrium geometry, in which width, depth, and slope adjust such that fluid stress slightly exceeds the threshold of sediment motion in the channel center and is at threshold on the channel banks [19–24]. This idea has not been tested on the multiple dynamic channels within a braided stream. The question of the statistics of channel network establishment was explored in a pioneering paper by Howard *et al.* [6], in which the authors showed that braided channel paths exhibit scaling relationships similar to those derived from random walk models. At a larger scale, diffusion has been invoked as a useful tool to model landscape evolution in a variety of field and laboratory settings, including braided river equilibrium profiles [20,21,25–28]. These macroscopic applications of diffusion to braided river evolution have not, however, been linked to underlying stochastic dynamics as in classical Brownian motion [29].

To address these open questions, we undertook a laboratory investigation of braided river evolution from an initially flat bed to a steady state (Fig. 1). Steady state for the purpose of this study was defined as establishment of the system equilibrium slope. Our experiments collected high temporal and spatial resolution data of topography (Fig. 2), allowing us to study the shape and kinematics of individual channels and the resultant network in detail. Our observations were used to motivate and test the following hypotheses: (1) individual channels fluctuate around an equilibrium geometry, dictated by near-threshold sediment transport; (2) the net effect of bank erosion, and bed scour and fill, is random lateral motion of channels; and (3) the dynamics are diffusive in nature, with estimates for diffusivity values consistent between the unit and system scale. Each of these hypotheses has a precedent, but they have not been linked together to describe braided river evolution. In this paper, we use several techniques to derive diffusivity values from the channel dynamics in our experimental braided rivers. We show how these dynamics map to a consistent diffusivity value at the system scale, and we propose that a diffusive framework has the potential to describe the kinematics of braided river evolution at all scales.

II. EXPERIMENTS

We describe the results of two experimental runs in which evolution was tracked from an initially flat bed of monodisperse glass beads (average diameter, $d_s = 0.261$ mm), in a tilted box of 1.5 m length and 0.75 m width. A constant input of water and sediment was introduced into the center of the upstream end, and the thin sheet of flow immediately carved a network of channels through bed load transport. All sediment arriving at the downstream end of the box was allowed to exit, and thus the initial slope of the granular bed was free to evolve to an equilibrium value. In the first run (R1), we took scans of topography and water depth at 5 min intervals for 6.7 h; methods are described in detail in Limare *et al.* [30]. This run had a constant incoming sediment discharge of $Q_s = 7.56 \times 10^{-8}\ \mathrm{m^3/s}$, water discharge of $Q_w = 5.00 \times 10^{-5}\ \mathrm{m^3/s}$, and tilted bed slope of $S = 2.1^\circ$. A second run (R2) was conducted to examine longer-time-scale dynamics

*mreitz@ldeo.columbia.edu

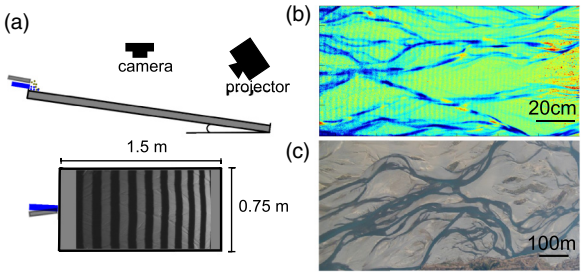

FIG. 1. (Color online) (a) Side view (above) and plane view (below) sketches of experimental apparatus. Water and sediment are fed into the top of a tilted rectangular bed. Overlain is an image of the sine wave fringe projected onto the braided river bed. (b) Water flow location data from a scan of the experimental braided river bed. Flow is from right to left of image. (c) Field example of a braided river in New Zealand. Photo taken by Greg O'Beirne, adapted with GFDL/Creative Commons permissions.

and had parameters similar to R1; $Q_s = 8.90 \times 10^{-8}\,\mathrm{m}^3/\mathrm{s}$, $Q_w = 3.33 \times 10^{-5}\,\mathrm{m}^3/\mathrm{s}$, and $S = 2.5^\circ$. Topographic scans for R2 were conducted at various intervals, ranging from 4 to 30 min, over a period of 22.7 h. In our analysis, data reported are from R1 unless otherwise noted, due to its higher continuous temporal resolution. Run R2 is used only for analysis requiring a longer-term data set. Though they represent only two experimental conditions of water and sediment flux, the objective here was to explore these individual runs in great detail in the context of quantifying diffusion, rather than to explore the sediment and water flux parameter space. The quantification of stochastic dynamics used averages over many measurements within a run. The system-scale measurements with only one data point per run were measures of the deterministic, macroscopic behaviors of diffusion and therefore should not be sensitive to the smaller-scale stochasticity.

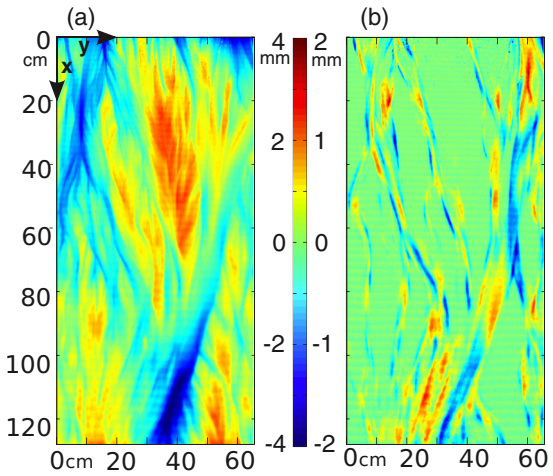

FIG. 2. (Color online) (a) A scan of the topography of the braided river, with flow in the x direction from top to bottom of the image. (b) The differenced topography between the scan in (a) and the scan taken 5 min later, giving a map of the erosion and deposition that has occurred in the interval.

Data output from the experiments was in the form of matrices of elevation and water depth for each camera pixel, at a resolution of 1 mm/pixel in the x-y direction, and $\sim$0.6 mm in the vertical (Fig. 2). To avoid edge effects near the inlet and outlet of the experimental table, we used a subset region of 0.82 m downstream by 0.61 m cross-stream area in the center of the table for our analysis. We first removed negative (nonphysical) values for water depth following the procedure of Limare *et al.* [30]. We then found empirically that isolating the third statistical quartile of depth values reliably identified flow locations. To isolate individual channels, we located each laterally continuous set of pixels along the y direction (cross-stream) identified as having flow. Because the y direction was not always perpendicular to channel flow, we included only channels whose primary flow direction was within 15° of the x axis. To determine the geometry of individual channels, we first fit a fourth-order polynomial to the dry topography data at the locations identified using the water depth data. The maximum and minimum in the second derivative of the polynomial were used to identify the curvature inflections that corresponded to the two channel banks. This method was used simply to make channel bank identification objective and repeatable; spot checks of the method revealed consistency with channel bank locations that would have been selected by eye. We chose a fourth-order polynomial because it was the lowest order able to capture the curvature inflection at both banks. We collected the raw channel geometry data between these points identified as the banks and then sorted these channel geometry data by width. All channels within a given scan having the same width were then averaged together, in order to counter effects of noise and obtain average channel geometry shapes.

Mean water depths of channels were $h \sim 1\,\mathrm{mm}$, and the mean total wetted width of a cross section was $W = 0.20\,\mathrm{m}$ (measurements taken for R1). This yields a water speed $u = 25$ cm/s and a Reynolds number of 250. This places our experiments in a transitional regime between laminar and turbulent flow [31]. Channels had Froude numbers of 2.5, which places them well into the supercritical regime. Natural braided rivers are fully turbulent; flood flows can be supercritical, but Froude numbers are typically closer to 1 [3]. However, the dynamics of channels relevant to evolution of the river system are insensitive to the modest influence that Reynolds and Froude numbers exert on time-averaged grain-scale transport [32–35]. More important is the dimensionless fluid shear (Shields) stress, which controls the mode and rate of sediment transport within the channels. Topography and water depth data allowed us to create maps of Shields stress [36] values (τ_*) at each point in a scan,

$$\tau_* = \frac{\sqrt{(hS/Rd_s)^2 + \sin^2\phi}}{\cos\phi}, \tag{1}$$

where $R = 1.65$ is the relative submerged density of the grains, S is the downstream slope, and $\tan(\phi)$ is the cross-stream slope at a given point. This version of the Shields stress formulation combines the downstream, fluid-driven shear and the cross-stream gravitational pull on the grains down the channel banks [36,37]. Using Eq. (1) and our channel geometry data, we measured and averaged Shields stress values across the channels.

III. EQUILIBRIUM CHANNEL GEOMETRY

Soon after the start of the experiment, channels were eroded into the initially flat granular bed. From mass conservation, the expected time to scour a channel scales like $hW^2/Q_s \approx 10^2$ s. We measured the trends of width-to-depth ratios with width and of the median ratio with time. To reduce noise, these measurements used a filter to only record ratio measurements where there were at least 10 channels of a given width in a given scan. We found that the median width to depth ratio of channels was established within a few scans and thereafter remained approximately constant, indicating relatively rapid achievement of equilibrium channel dimensions (Fig. 3). The scaling of channel width to depth ratios with width was also approximately constant for all scans (Fig. 3 inset), with a median value of $W/h = 53$. The median ratio may exhibit a slight decline through time and a slight increase with width. However, either case of a constant ratio or a ratio that scales in a consistent manner supports the idea of a channel equilibrium that organizes on time scales rapid relative to the system-scale organization, which is the condition we have described as a prerequisite for the diffusion approach. Previous work by Foufoula-Georgiou and Sapozhnikov [9] focused on the scaling among individual channels of different size and found dynamic scaling in time that they interpreted as being due to a self-organized critical behavior. Though the types of measurements taken in those experiments and ours were different and comparison of the results is not straightforward, the connection of our observed self-similarity in channel width-to-depth ratios with the dynamic scaling of channel size in those experiments is an open and interesting question for future research.

Shields stress values [Eq. (1)] were computed at each location across each channel, and we found a common pattern across the range of channel sizes observed. As illustrated in Fig. 4, average instantaneous Shields stress values were approximately constant with a value $\tau_* \sim 0.06$–0.08 across most of the channel, with a decline at the outer margins

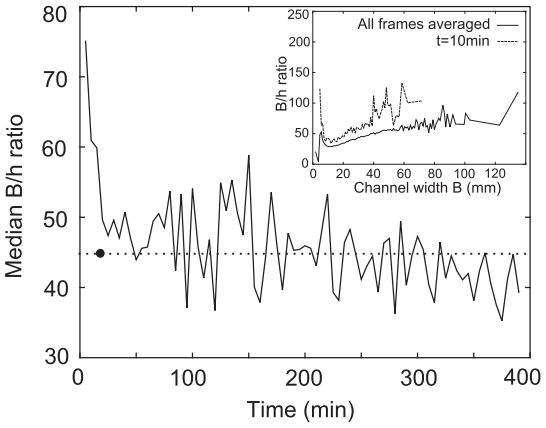

FIG. 3. Trend of median channel width-to-depth ratio with time for R1 (solid line). The dotted line guides the eye to show the constant nature of the ratio, and the black circle on this line marks the approximate time at which the channels have attained equilibrium. Inset: Trend of width-to-depth ratio with channel width, for all channels averaged (solid line) and for an early snapshot of ratio establishment at 10 min into the run (dashed line).

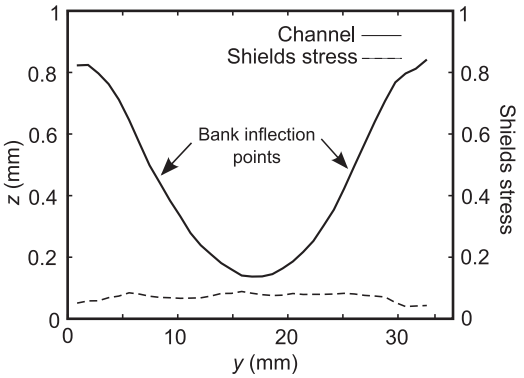

FIG. 4. An example profile of the channel geometry, with y as the cross-stream and z as the vertical coordinates, together with the Shields stress profile. The profiles are the average of all ~100 of the cross-stream profiles of Shields stress and channel geometry for this given width within a scan. The widths averaged fell within the range of an individual pixel's width of 0.93 mm.

to a slightly lower value. Assuming the threshold Shields stress for our experiments to be approximately $\tau_{*c} = 0.05$, a commonly reported value [20–22,38], the calculated Shields stress in the channel center was on average higher than threshold by a factor of approximately $\tau_* = 1.3\tau_{*c}$. These results are consistent with theory and field measurements for single-channel gravel rivers, which found a narrow range for the prefactor of 1.2–1.4 [19–21]. The measured channel width-to-depth ratio is also consistent with the theory, and with field and experimental observations [24]. Although individual channels in the braided river are constantly changing shape through scour and fill, these appear to be fluctuations around a robust equilibrium geometry that becomes apparent when many individual channel geometries are averaged together.

IV. TRANSIENT CHANNEL DYNAMICS AND STOCHASTIC DIFFUSION

In a diffusive system, the unit-scale process exhibits random behavior. In the diffusion of heat, for example, the individual gas atoms exhibit random motion; in the case of this braided river system, the random movement would be exhibited by the ephemeral channel migration dynamics. This random motion can be characterized by an exponential decay of correlation in channel position F, with a decay constant that depends on the system diffusivity ν and the selection of an appropriate length scale for the process, L:

$$F = \exp(-t/T_c), \tag{2a}$$

$$\text{where } T_c \sim \frac{L^2}{\nu} \tag{2b}$$

Also, the rate of growth of correlation length scales L_e in a diffusive system is expected to scale with the square root of time, with a prefactor that depends on the system diffusivity:

$$L_e \sim \sqrt{\nu t}. \tag{3}$$

We tested the applicability of diffusion to our experiments by quantifying the channel motion and the transient growth of

correlation length scales, and comparing our results to Eqs. (2) and (3).

Channel migration in the (y) direction transverse to flow occurred due to bank erosion and/or in-stream deposition [5,15]. Flow expansions and channel mergers created migrating zones of deposition and erosion [11,17], respectively, with the net effect of driving longitudinal (x direction) channel migration [Fig. 2(b)]. For this study, we did not quantify specific drivers of channel change, such as the formation and migration of midchannel bars, but rather measured the net effect of these processes on channel movement. We quantified this rate of channel change by assessing the rate of change in the two-dimensional (2D) (x-y) pattern of flow occupation. For this measurement, we first created maps of the 2D flow locations for all scans. Then, starting from a given frame, we computed the percent of these flow locations that were still occupied at the next time step. We then repeated this measurement for all subsequent time steps, to measure the decay in the percent of continuously occupied wetted area, which we termed the wet fraction decay (F). We quantified this decay using the flow location map at each frame as a starting point, and then averaged these measured decays. The final averaged wet fraction decay is plotted in Fig. 5(a).

We tested the hypothesis that channel migration in our experiments can be characterized by a random process by fitting Eq. (2) to the measured wet fraction decay in our experiments. For application of Eq. (2), we estimated the appropriate length scale of the wet fraction to be the square root of the average wetted area, or $L^2 = A_w = 0.13\,\mathrm{m}^2$. We confirmed that the decorrelation in channelized area had an exponential form [Fig. 5(a)], an indication that channel migration in this system is effectively a random process at this coarse-grained scale. The fit yielded an estimate for T_c, the characteristic time scale that describes the decay of the wet fraction to a value of $1/e$ (the characteristic length of the exponential), of $T_c = 565\,\mathrm{s}$, and a corresponding estimate for diffusivity of $\nu \sim 10^{-4}\,\mathrm{m}^2/\mathrm{s}$. The parameter ν is the diffusivity value that will connect this unit-scale process to the system scale.

Although individual channel widths and depths achieved equilibrium scaling soon after the start of the experiment, the structure of the system topography took more time to develop. As channels carved the initially flat surface and migrated, the topography began to develop longer correlation lengths in the downstream direction due to the development of new and relict coherent channels. We quantified this developing structure in the channel network by examining topographic correlations. In order to measure the spatial autocorrelation of topography in the downstream (x) direction through time, for each cross-stream row of topography data, we computed the decline in the correlation coefficient (the R value) between this row and subsequent rows downstream. This analysis was conducted for run R2, as R1 did not have sufficient data to assess a long-time trend. We then averaged these declines in correlation for each scan and fitted the average decay of correlation for each scan with an exponential function. We defined the correlation length, L_e, as the length scale at which the correlation coefficient has fallen to $1/e$ (the characteristic length of the exponential). We tracked the evolution of L_e through time [Fig. 5(b)].

Because our channel decorrelation data indicated that the channel migration dynamics are random, we expect the rate of development of the channel-carved topography to be diffusion limited, such that the topographic correlations L_e will follow the scaling of Eq. (3). We fitted the growth of L_e against the square root of time and found a relationship consistent with this diffusional scaling, $L_e = 5 \times 10^{-3}\, t^{0.5}$ ($R^2 = 0.78$) [Fig. 5(b)]. If we assume that the downstream e-folding correlation length is representative of the system, we can use the coefficient of Eq. (3) to obtain an estimate for diffusivity of $\nu \sim 10^{-5}\,\mathrm{m}^2/\mathrm{s}$. This simplifying assumption neglects, however, a likely distinction between cross-stream and down-stream topography correlation, so although we report the estimate for completeness, we will not rely on it for direct comparison to diffusivity values derived for R1. The square-root scaling of

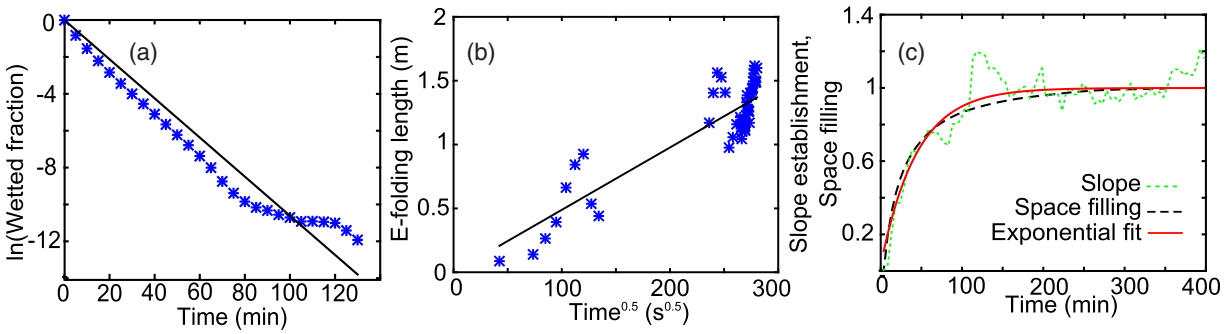

FIG. 5. (Color online) Dynamical estimates of diffusivity. (a) Decorrelation of wet fraction with time (asterisks), plotted in ln-linear space with the best-fit exponential decline (solid line); straight line correspondence supports the behavior as exponential. Diffusivity estimated using Eq. (2). (b) Growth of the downstream correlation length of topography for R2 (asterisks), plotted against the square root of time (solid line); best-fit line yields an estimate of diffusivity [Eq. (3)], while the fit of a straight line confirms the diffusive square root of time scaling. (c) Overlain plots of downstream slope as its equilibrium value is established during the experiment ("slope establishment," light green dotted line) and the increase in the cumulative fraction of the surface visited by water (space filling) for R1 (black dashed line), each normalized to their initial and final equilibrium values. Also plotted is the exponential fit to slope establishment data (solid red line), which allows an estimate of diffusivity in a similar manner to (a).

correlation length scale with time is, however, consistent with diffusion.

V. SLOPE EVOLUTION AND DETERMINISTIC DIFFUSION

Diffusive systems are characterized at the macroscopic scale by a deterministic equation in which the flux of a quantity (such as heat) is proportional to the spatial gradient of this quantity. Following previous authors [27], we hypothesize that the macroscopic flux of sediment resulting from the random motion of individual channels is proportional to the downstream slope of the river:

$$Q_s = \nu S W. \tag{4}$$

When combined with mass conservation, Eq. (4) yields the diffusion equation that describes the evolution of bed topography. This deterministic formulation is expected to apply to time and space scales significantly larger than those associated with individual channel dynamics.

When a diffusive system is out of equilibrium, the transient process of its approach to the equilibrium state can be described with an exponential decay equation of the form of Eq. (2). The appropriate length scale in Eq. 2(b) changes to the length scale of the entire channel system, but the diffusivity value should be consistent.

We tested whether the above diffusive relationships held within our braided river system. First, we tested the macroscopic relationship from Eq. (4) using our input flux and the measured equilibrium slope $S = 0.039$. We estimated this macroscopic diffusivity in our experiment to be $\nu \sim 10^{-5}\,\mathrm{m}^2/\mathrm{s}$, consistent with estimates derived from stochastic channel migration.

Next, we tested whether the transient adjustment of the slope followed the theory for the rate of approach to equilibrium. We found the adjustment of bed slope through time was well fitted by the expected exponential form of Eq. (2), with a characteristic (e-folding) time of $T_s = 2650$ s [Fig. 5(c)]. Because slope adjustment involves regrading the entire channel system, we took the appropriate length scale in Eq. 2(b) to be the square root of the total area of the braided river system, or $L^2 = 1.125\,\mathrm{m}^2$. The computed diffusivity using these numbers from the slope adjustment time was $\nu \sim 10^{-4}\,\mathrm{m}^2/\mathrm{s}$.

Finally, to connect the macroscopic adjustment time scales with the channel migration dynamics, we quantified the rate at which channels cumulatively filled space. Starting with the 2D flow map of a given frame, we measured the increase in subsequent frames of the percentage of the surface that had ever seen occupation by water, and we averaged the space-filling trends starting from each frame. We found that the form of this rate at which channels filled space tracked the river equilibrium slope establishment. This correspondence indicates that the time scale for the channels to visit the entire surface dictates the rate at which the equilibrium slope is established [Fig. 5(c)]. As the channels migrated over the surface, they established the equilibrium slope through their own internal organization of channel width, depth, and slope to the conditions of water and sediment flux.

VI. DISCUSSION AND CONCLUSIONS

Two basic tenets, that individual channels are threshold equilibrium channels, and that they fill space by random migration, are sufficient to describe the spatiotemporal dynamics of our experimental braided river from channel to network scale, within the context of diffusion. Channels are coherent units with long correlation lengths in the downstream direction that link together to form a complex network (Fig. 2). Yet the motion of these channels is effectively random at the coarse-grained scale and results in net diffusional behavior. Our findings represent the first time that a unit process, such as stochastic channel movement, has been directly mapped to landscape-scale diffusion in an experiment, although such mapping has been anticipated by theory [39–41]. The applicability of diffusion requires three key conditions, all supported by our experimental observations: (1) the time scale of channel formation is significantly smaller than the time scale of network evolution; (2) channel shape, although variable in time, fluctuates around a well-defined geometry; and (3) channel motion has no memory; i.e., there are no preferred channel locations and there is no strong attraction or repulsion of interacting channels.

The numerical model results of Murray and Paola [2] suggested that the fundamental instability that induces braiding is the nonlinear dependence of sediment transport on fluid shear stress, which results in amplification of erosion at channel confluences and deposition at channel bifurcations. More than 40 yr ago, Howard *et al.* [6] hypothesized that the net effect of these processes playing out across a spatially extended landscape would be diffusion. Our results support this hypothesis. The four independent empirically derived diffusivity values from channel migration and slope adjustment in our experiments are consistent within one order of magnitude. There is some scatter in the computed values, but the general agreement is encouraging. It suggests a need for a comprehensive theoretical underpinning for the application of statistical diffusion to braided river systems, which will provide a path forward for extending and applying these findings to natural rivers. With knowledge of basic variables measured from the field, one could make predictions about expected scour depths and migration rates of channels, and the time required for a braided river to visit an entire valley floor. Such predictions would aid in the assessment of many societally useful quantities, such as erosion and flooding risk.

ACKNOWLEDGMENTS

We are grateful for funding through an NSF Critical Zone grant to T. White. We are also grateful to H. Bouquerel, Y. Gamblin, T. Rivet, and A. Vieira for building the experimental setup and developing the measurement methods.

[1] A. D. Miall, Earth-Sci. Rev. **13**, 1 (1977).
[2] A. B. Murray and C. Paola, Nature (London) **371**, 54 (1994).
[3] P. J. Ashworth, J. L. Best, and M. A. Jones, Sedimentology **54**, 497 (2007).

[4] F. Métivier and L. Barrier, in *Gravel-Bed Rivers: Processes, Tools, Environments*, edited by M. Church, P. M. Biron, and A. Roy (Wiley-Blackwell, New York, 2012), pp. 474–501.
[5] P. J. Ashworth, Earth Surf. Proc. Landforms **21**, 103 (1996).
[6] A. D. Howard, M. E. Keetch, and C. L. Vincent, Water Resour Res. **6**, 1674 (1970).
[7] S. A. Schumm and H. R. Khan, GSA Bull. **83**, 1755 (1972).
[8] V. B. Sapozhnikov and E. Foufoula-Georgiou, Water Resour. Res. **35**, 843 (1999).
[9] E. Foufoula-Georgiou and V. Sapozhnikov, Math. Geol. **33**, 273 (2001).
[10] P. Ashmore, Can. J. Civ. Eng. **36**, 1656 (2009).
[11] W. Bertoldi, L. Zanoni, and M. Tubino, Earth Surf. Proc. Landforms **34**, 547 (2009).
[12] Y. Fujita, in *River Meandering*, Vol. 12, edited by S. Ikeda and G. Parker (AGU, Washington, D.C., 1989), pp. 417–462.
[13] G. Parker, J. Fluid Mech. **76**, 457 (1976).
[14] S. Ikeda, G. Parker, and K. Sawai, J. Fluid Mech. **112**, 363 (1981).
[15] P. Blondeaux and G. Seminara, J. Fluid Mech. **157**, 449 (1985).
[16] R. Luchi, G. Zolezzi, and M. Tubino, Earth Surf. Proc. Landforms **35**, 902 (2010).
[17] I. A. Lunt, J. S. Bridge, and R. S. Tye, Sedimentology **51**, 377 (2004).
[18] W. Bertoldi and M. Tubino, Water Resour. Res. **43**, W10437 (2007).
[19] G. Parker, J. Fluid Mech. **89**, 127 (1978).
[20] G. Parker, C. Paola, K. Whipple, and D. Mohrig, J. Hydraul. Eng.-ASCE **124**, 985 (1998).
[21] G. Parker, C. Paola, K. Whipple, D. Mohrig, C. M. Toro-Escobar, M. Halverson, and T. W. Skoglund, J. Hydraul. Eng.-ASCE **124**, 996 (1998).
[22] G. Parker, P. R. Wilcock, C. Paola, W. E. Dietrich, and J. Pitlick, J. Geophys. Res. **112**, F04005 (2007).
[23] W. B. Dade and P. F. Friend, J. Geol. **106**, 661 (1998).
[24] G. Seizilles, O. Devauchelle, E. Lajeunesse, and F. Métivier, Phys. Rev. E **87**, 052204 (2013).
[25] W. E. H. Culling, J. Geol. **68**, 336 (1960).
[26] Z. B. Begin, D. F. Meyer, and S. A. Schumm, Earth Surf. Proc. Landforms **6**, 49 (1981).
[27] C. Paola, P. L. Heller, and C. L. Angevine, Basin Res. **4**, 73 (1992).
[28] M. W. I. M. van Heijst, G. Postma, X. D. Meijer, J. N. Snow, and J. B. Anderson, Basin Res. **13**, 243 (2001).
[29] A. Einstein, Ann. Physik **17**, 549 (1905).
[30] A. Limare, M. Tal, M. D. Reitz, E. Lajeunesse, and F. Métivier, Solid Earth **2**, 143 (2011).
[31] J. P. Peakall, P. Ashworth, and J. Best, in *The Scientific Nature of Geomorphology*, edited by B. L. Rhoads and C. E. Thorn (John Wiley and Sons, New York, 1996), pp. 221–253.
[32] C. Paola, K. Straub, D. Mohrig, and L. Reinhardt, Earth-Sci. Rev. **97**, 1 (2009).
[33] L. Malverti, E. Lajeunesse, and F. Métivier, J. Geophys. Res. **113**, F04004 (2008).
[34] E. Lajeunesse, L. Malverti, P. Lancien, L. Armstrong, F. Métivier, S. Coleman, C. E. Smith, T. Davies, A. Cantelli, and G. Parker, Sedimentology **57**, 1 (2010).
[35] E. Lajeunesse, L. Malverti, and F. Charru, J. Geophys. Res. **115**, F04001 (2010).
[36] O. Devauchelle, A. Petroff, A. Lobkovsky, and D. Rothman, J. Fluid Mech. **667**, 38 (2011).
[37] F. M. Henderson, J Hydraulics Div, ASCE **87**, 109 (1961).
[38] J. M. Buffington and D. R. Montgomery, Water Resour. Res. **33**, 1993 (1997).
[39] D. J. Furbish and P. K. Haff, J. Geophys. Res. **115**, F03001 (2010).
[40] E. Foufoula-Georgiou, V. Ganti, and W. E. Dietrich, J. Geophys. Res. **115**, F00A16 (2010).
[41] G. E. Tucker and D. N. Bradley, J. Geophys. Res. **115**, F00A10 (2010).